Nuclear Technology (2023) DOI: 10.1080/00295450.2023.2173482

Analysis and preliminary design of Primary Heat Exchanger failure testing facility for Lead-cooled Fast Reactors

Federico Hattab,[a]* Fabio Giannetti,[a] Vincenzo Narcisi[a], Pierdomenico Lorusso[b], Filippo Bussoletti[c], Michael Epstein[d], Sung Jin Lee[d], Mariano Tarantino[e]

[a] *"Sapienza" University of Rome, DIAEE – Nuclear Section, Rome, Italy*

[b] *ENEA, Department of Fusion and Nuclear Safety Technology, Frascati, Italy*

[c] *S.R.S. Servizi di Ricerche e Sviluppo srl, Rome, Italy*

[d] *Fauske and Associates, LLC., Bolingbrook, Illinois*

[e] *ENEA, Nuclear Safety, Sustainability and Security Division, Bologna, Italy*

*E-mail: federico.hattab@uniroma1.it

Nuclear Technology (2023) DOI: 10.1080/00295450.2023.2173482

Analysis and preliminary design of Primary Heat Exchanger failure testing facility for Lead-cooled Fast Reactors

This paper presents an assessment aimed at evaluating the Primary Heat Exchanger (PHE) failure of the Westinghouse Electric Company (Westinghouse) Lead-cooled Fast Reactor (LFR) and at designing a facility for testing the phenomena involved in the failure. The system thermal-hydraulics code RELAP5/MOD3.3 was used to develop a transient analysis simulation at reactor scale. Due to the inability to mix working fluids in the RELAP5/MOD3.3 code, the steam injection effect was evaluated using the SIMMER-III code. Limits and strengths of both codes are highlighted throughout the paper. Reactor-scale steady state results are in good agreement with the nominal operating condition. The transient results show that the lead pool surface level variation and primary system pressurization during the PHE failure event are limited.

The PHE failure testing facility was characterized, and a preliminary layout was developed. The separate effect transient inside the vessel was analysed with SIMMER-III and RELAP5/MOD3.3 runs. The simulation outcomes have provided useful data to inform subsequent design stages for the test facility. Different configurations of the facility have been assessed, highlighting strengths and weaknesses of each design. The most important issue was identified to be the lead pool swelling, reaching the vessel's lid and blocking the pressure relief vent. This poses a safety hazard that must be addressed and has been raised for resolution in subsequent design stages. The so-called V4 configuration is suggested as a starting point for further improvement of the facility. Furthermore, a smaller failure opening and lower lead level in the vessel are suggested.

Keywords: RELAP5, sH2O, Westinghouse LFR, SIMMER, Printed Circuit Heat Exchanger

I. INTRODUCTION

Among the Generation IV International Forum (GIF) reactor technologies, the Lead-cooled Fast Reactor (LFR) is considered to be one of the best choices for near term deployment (first unit by 2035 – 2040) (Ref. 1). Currently, the efforts of the European Union (EU) are being directed mainly towards three LFR designs: MYRRHA

(Multi-purpose hYbrid Research Reactor for High-tech Applications)[2], a subcritical lead-bismuth eutectic cooled research reactor, ALFRED (Advanced Lead Fast Reactor European Demonstrator)[3][4], the EU LFR demonstrator, and SEALER (Swedish Advanced Lead Reactor), a compact reactor for arctic environments and on-grid applications[5].

BREST-OD-300 is the pilot LFR demonstrator proposed by the Russian Federation, for which licence for construction was issued by the Russian nuclear regulator on 10th of February 2021 (Ref. 6), first concrete was poured in June 2021 and foundation slab was completed in November 2021 (Ref. 7).China is mainly working on CLEAR, a lead-based ADS reactor[8].

In the United States of America (USA) Westinghouse Electric Company (Westinghouse) is developing a ~450 MWe LFR and is collaborating with international organizations toward this goal. Specifically, key development activities are being performed in the United Kingdom (UK) as part of Phase 2 of The Advanced Modular Reactor Program funded by the UK Department for Business Energy & Industrial Strategy (BEIS). In this program, Westinghouse and its partners are installing eight test facilities in the UK, aimed at demonstrating key materials, systems, components, and phenomena of the Westinghouse LFR. Operation of these test facilities is anticipated to occur in second half of 2022. These facilities support Westinghouse strategy for reactor deployment which features separate effect tests supporting development of a near-term demonstration plant planned by early 2030s, followed by a First Of A Kind (FOAK) unit of a commercial fleet expected to be deployed in the second half of 2030s.

The objective of this work is primarily the simulation of the Primary Heat Exchanger (PHE) failure in the Westinghouse LFR. The expected outcome is to acquire useful information for the design and realization of a dedicated test facility for studying the phenomena involved in the PHE failure. This facility is part of the network of facilities mentioned above as is designed for installation at the Westinghouse location in Springfields, UK. To investigate the facility's performance, two computational tools have been used: RELAP5/MOD3.3 (Ref. 9) and SIMMER-III code (Ref. 10). These two codes have strengths and weaknesses, which have been taken into consideration and justified the use of both codes for the purpose of this investigation. On one hand, RELAP5/MOD3.3 is a system thermal-hydraulic code largely used for the licensing of nuclear reactors (well validated for Light Water Reactors), but it does not allow more than one working fluid (the computational domain allows only one working fluid plus non-condensable gases). On the other hand, SIMMER-III can simulate interaction of two fluids (e.g., lead and water) but its application is limited due to computational cost, memory usage, and nodalization scheme (which favours axisymmetric geometries). For this reason, a preliminary SIMMER-III run was performed to identify equivalent non-condensable (NC) conditions to simulate water injection in lead with RELAP5/MOD3.3.

The activity described in this paper is the result of a collaboration between the Department of Astronautical Electrical and Energy Engineering (DIAEE) of Sapienza University of Rome and the Italian National Agency of New Technologies, Energy and Sustainable Economic Development (ENEA). To provide realism and ensure value for this work, the analysis on LFR has been developed leveraging a collaboration with Westinghouse and its partner organizations, as part of the UK BEIS program mentioned above. As such, the characteristics of the LFR discussed in this document are broadly in line with the Westinghouse LFR design[11]. However, no quantitative data presented in this study (either input data or analysis results) should be taken as reference for the actual design or performance of any previous, current, or future Westinghouse LFR.

Since this is a first-of-a-kind facility it is not expected to capture every relevant aspect of the design before doing any experiment. Based on first experimental results, improvements in the design of the facility are planned.

II. THE WESTINGHOUSE LEAD COOLED FAST REACTOR

The Westinghouse LFR is a highly simplified, passively safe, scalable LFR (Ref. 11, 12). It is a pool type reactor with three PHEs and three Reactor Coolant Pumps (RCPs). The lead pool is generally analysed as comprised of three sub-pools; the Hot Pool (HP) contains hot lead exiting the core, while the Upper Cold Pool (UCP) and Lower Cold Pool (LCP) contain cold led downstream PHEs exits and after the RCPs, respectively. As shown in Figure 1, the lead coolant exiting the core enters the HP and then flows radially through windows in the wall of the core barrel into the PHEs. Cold lead enters in the UCP, where the pumps intakes collect the coolant and move it from the UCP to the LCP. The PHEs are hybrid Printed Circuit Heat Exchangers (PCHEs), a technology which provides a highly compact structure while ensuring a very strong construction thanks to the diffusion bonding manufacturing process (they are capable of withstanding pressures in excess of 1000 bar, depending on the temperature[13]) and the small size of the (pressurized) secondary coolant channels. The PHE are composed of flat metal plates with chemically etched flow channels. Such plates are joined together by diffusion bonding to make a heat exchanger block. In the PHE the secondary coolant channels are U-shaped and contain the secondary fluid SuperCritical Water (SCW), which enters and exits from the top. Columns of primary and secondary channels are alternated along the length of the component. A notational representation of the heat exchanger is shown in Ref. 12. Moreover, in the Westinghouse LFR the secondary headers are located outside of the reactor vessel in order to limit the size of potential in-vessel secondary side breaks to microchannels, as to minimize break flow rate and thus the consequences of this event.

[FIGURE 1 GOES HERE]

Table I shows key input data used for the simulations presented in Section 4.

[TABLE I GOES HERE]

III. THE WESTINGHOUSELEAD-COOLED FAST REACTOR PRIMARY HEAT EXCHANGER FAILURE

In this Section an overview of the current status of PCHE is presented, followed by an analysis of the PHE failure phenomenon and a presentation of experimental evidence in the injection of water into molten metals.

III.A. PCHE State of the Art

Because of PCHEs compactness, high thermal effectiveness, and low pressure drops, interest in them is increased in advanced nuclear reactors[14]. Nevertheless, even though PCHEs have been widely used in the oil and natural gas industry in the last two decades, the nuclear power industry is yet to adopt this technology[15].

PCHEs have been rated to operate under temperatures ranging from cryogenic to 900°C and to withstand pressures up to 60 MPa (Ref. 16). However, due to these extreme conditions, they require more detailed thermal and mechanical analysis compared to conventional heat exchangers[17].

In nuclear reactor systems, PCHE could be as important as a "safety-related" component due to its boundary function of the reactor coolant system, and its design reference construction code is the ASME BVPC Section III (Ref. 18). Three variables play an important role in the diffusion bonding process: the bonding temperature, the bonding pressure, and the holding time[19]. The bonding temperature and pressure should be adequately lower than the parent metal absolute melting point and the material yield strength, respectively[20]. Due to the high temperature and pressure differentials anticipated in the proposed nuclear applications, careful design is required in order to ensure that internal stresses do not cause flow passage deformation and/or failure[21].

According to studies on PCHE structural integrity[18][22][23][24], the mechanical stress concentration in PCHEs occurs at the tip edge of the channel and the increase of channels misalignment causes an increase in stress intensity. This leads to the increase of the utilization factor and, therefore, to a less safe condition. As long as the local stress concentration is lowered sufficiently thanks to plasticity, PCHEs made of SS316 are expected to comply with ASME standards[22].

According to Vacuum Process Engineering (VPE) (Ref. 25) tensile tests, diffusion bonds can have strengths close to the one of the base metal. The integrity of diffusion bonded PCHE cores enables them to withstand pressures more than 10 times their design pressure[19]. A demonstration of their capability to retain a high pressure fluid is presented by the destructive test performed by Aakre et al.[19].

As reported by Dostal et al.[26], the probability of a leak is very low and if the leak occurs it is very small, with the most likely failure mechanism being fatigue, especially where a control mechanism that rapidly turn on/off the device is employed (unlikely in nuclear reactor applications). Up to the time of Dostal's publication, Heatric, the world's largest PCHE manufacturer[27], did not have a single failure of the headers[26].

Should small crack(s) or micro-leaks occur, the secondary fluid could bleed into the primary system at a relatively low rate. This kind of failure mode was observed in PCHEs used in the offshore oil and gas industry[28]. A severe jet blowdown is more relevant in shell-and-tube heat exchangers, which do not have solid block construction and the channel size (and thus break flow rate) is much larger than in PCHE (Ref. 28).

In this work, one-channel and three-channel failure scenarios are considered for safety analyses of the Westinghouse LFR. Based on the reported experimental evidence, one-channel and especially three-channel failure are deemed highly unlikely. Nonetheless, the phenomenology and impact of the transient need to be better understood. For each failed channel, a rupture flow area equal to two times the secondary channel flow area is considered, to account for the fluid flow from both sides of the rupture. These assumptions define the boundary conditions for the reactor scale failure analysis presented in this paper.

III.B. PHE failure phenomenology

In this section the PHE failure event analyzed by Epstein[29] and an overview of existing experimental evidence of water injection into liquid lead are presented. Furthermore, the risk of steam explosion following the rupture event evaluated by Epstein[30] is presented.

With reference to the Westinghouse LFR PHE, following channel rupture a blowdown of a two-phase mixture from high-pressure secondary side into primary lead takes place. Pressure waves propagate from the failure location to the surrounding HP and UCP. Lead is expelled from the PHE primary side channels involved in the failure and, from the same channels, a two-phase water blowdown takes place. Both streams impinge on adjacent structures and reaction forces are exerted from the PHE itself. Due to the blowdown liquid lead sloshing is expected. Beyond loads on structures/components and sloshing, other possible phenomena associated with the failure are migration of bubbles to the core region, steam explosions and release of aerosol to the cover gas region, enhanced by the water flow. The latter represents a release mechanism of fission products dissolved in liquid lead. The risk of steam inlet inside the core is reduced by the high density of the coolant[31].

When the rupture happens, there is a step change in pressure across the failure opening, from P_o, that is the water pressure in the secondary loop, to P_∞, the hydrostatic lead pressure at that point (Figure 2). Assuming an ideal behaviour, two planar shock waves travelling in opposite directions are generated. Let us consider one of the two planar shock waves. Conservatively, a planar shock wave of strength P_o, along with a liquid velocity u_s behind it, is considered (item 1 in Figure 2). The assumption of P_o is conservative because, due to the compressibility of the two fluids, the shock pressure value should be between P_o and P_∞.

[FIGURE 2 GOES HERE]

Once the end of the channel is reached, the planar shock wave spreads in a hemispherical shock wave of radius R (see item 2 in Figure 2). Then, the shock wave propagates radially as a spherically symmetric water hammer. The maximum pressure on the wall is exerted at the minimum distance r = S between the wall and failure opening. It can be obtained by considering the pressure field P(r,t) and velocity filed u(r,t) behind the spherically symmetric water hammer, given by a revised derivation of Moody[32], and using the superposition principle for solutions of linear partial differential equations in conjunction with the virtual images method.

Let us consider the risk of lead being pushed on the RV wall following the failure event. If $\dot{m}$ is the liquid lead mass flow rate, the momentum equation of the liquid lead plug when it is displaced for a distance x after a time t is:

$$\frac{\mathrm{dmu}}{\mathrm{dt}} = (P_{ch} - P_\infty)A_{pr} + \dot{m}u \qquad (1)$$

Where A_{pr} is the cross-sectional area of the PHE primary channel, m is the lead mass, u is the lead velocity, and P_{ch} is the pressure in the channel.

In Eq. (1) the channel is assumed frictionless, a conservative condition since friction reduces the lead expulsion velocity. The lead expulsion from the ruptured channel can be modelled as an interrupted high momentum jet driven by the secondary fluid blowdown pressure until the time at which the lead expulsion is terminated. From the momentum jet theory, the distance S_p at which the jet penetrates the lead pool is:

$$S_p = \left(\frac{r\bar{u}t_{ex}}{E_0}\right)^{\frac{1}{2}} \tag{2}$$

Where E_0 is an empirical entrainment coefficient (approximate value = 0.08), r is the channel radius, $\bar{u}$ is the average jet release velocity, t_{ex} is the lead expulsion time, L is the length of the PHE primary channel, and $\bar{u}$ is specified in Eq. (3).

$$\bar{u} = \frac{L}{2t_{ex}}\,(\text{middle failure}), \quad \bar{u} = \frac{L}{t_{ex}}\,(\text{end failure}) \tag{3}$$

By plugging $\bar{u}$ from Eq. 3 into Eq. 2 and with the primary channel geometry considered in this study, it is found that the lead jet penetrates radially up to 0.122 m for a middle failure and up to 0.172 m for an end failure. Both distances are less than the distance between the PHE outlet and the vessel wall, thus the lead plug is not expected to impinge directly onto the vessel wall.

Another phenomenon that deserves investigation is the sloshing of the lead pool due to the continuous secondary fluid discharge. Initially, the two-phase mixture travels horizontally. Then, it gradually moves upward due to the jet buoyancy, and in its motion entrains the surrounding lead. An alternative possible mechanism is that instead of rising in a coherent manner, the jet breaks up into bubbles. The momentum of the rising mixture causes the lead pool surface to rise and the formation of waves impinging the various structures immersed in the HP and UCP (i.e., PHE walls, reactor coolant pump shafts, core barrel, and control rod drivelines) and on the reactor vessel wall. The magnitude of such sloshing motion was assessed in the computational campaign presented in Chapter IV, and found to be very small.

III.C. Existing experimental evidence of water injection in liquid lead

Table II shows a summary of the key parameters of the experiments analyzed in this paper.

[TABLE II GOES HERE]

Water at 340 °C and 350 bar passing through a small opening will in part vaporize and in part condense due to the much lower pressure on the lead side[33][34]. Experimental and theoretical results confirm that the injected water stream breaks up due to boiling and interaction with the liquid lead coolant.

Beznosov et al.[35] conducted an experimental and theoretical study on water and steam injection inside a liquid lead column. The heat transferred during contact can be significantly more than the amount of heat transferred through the wall because the heat transfer surface can increase by a large degree when the vapor layer breaks up[35].

Three experimental campaigns, briefly discussed below, were conducted in the facility LIFUS5 (see Figure 3) at ENEA Brasimone (Italy), involving injection of water into a Lead Bismuth Eutectic (LBE) pool to study postulated LFR Steam Generator Tube Ruptures or leaks. The main components of the facility are an interaction vessel (S1A) connected to a dump vessel (S3) and a water tank (S2V) which stores the fluid to be injected.

[FIGURE 3 GOES HERE]

An experimental and SIMMER-III computational campaign has been performed by Ciampichetti et al.[36] on the LIFUS5 facility. The computed temperature and pressure trends have shown remarkable analogies with the experimental trends. However, a delay in reaching the maximum pressure in S1, and a smoother "depressurization phase" in both S1A and S3 were observed. This was due to the geometrical simplifications adopted in the computational domain.

In the experimental campaign conducted by Del Nevo et al.[37] a special injection line was tested in the LIFUS5 facility, characterized by an end cap provided with a notch designed to rupture at a predetermined pressure. A sudden water phase change caused a pressure increase within S1 and the flow of a mixture of LBE-vapor-argon into S3. Overall, water injection was found to result into low strain values measure in S1A, comparable with those resulting from experiments conducted at lower water pressure. It was found that the various elements of the test section helped damping the pressure waves.

Eboli et al.[38] investigated water-LBE interaction resulting from postulated cracks (rather than from orifices). Water was injected through a plate with a laser cut hole and the injection system was designed with a replaceable injector device. A RELAP5/MOD3.3 analysis was performed to evaluate the mass flow rate at the simulated crack. The interface between S1A and S3 was modelled as an imposed temperature (200 °C) and pressure (1.1 bar) boundary condition. Heat transfer between LBE and water was not simulated. Simulation results showed a mass flow rate drop as the water was heated up to 200 °C and its temperature got closer to the saturation temperature; with increasing water temperature two-phase choked flow was established.

III.D. Steam explosion

Steam explosion is a violent fuel-coolant interaction with a significant amount of steam generated and exploded. When high-temperature liquid comes into contact with a colder volatile liquid, violent interactions are observed[39]. The potential for steam explosion must therefore be addressed in the safety analysis of LFR system since it could cause damages within the reactor vessel. It should be noted, however, that none of the experiments reviewed so far, in which subcooled water at high pressure was injected inside a lead or LBE pool, showed evidence of a steam explosion. Some key results from the evaluation of steam explosion due to accidental supercritical liquid water discharge from PHE into molten lead pool conducted by Epstein[30] is presented here.

Sibamoto et al.[40] experimentally investigated the effect of a subcooled water jet at ambient pressure vertically injected onto the surface of an LBE pool. The authors reported an energetic interaction between the two fluids. Specifically, when the instantaneous interfacial temperature was greater than the minimum film boiling temperature, an explosive boiling occurred, resulting in the damage of the 1 mm thick stainless steel test section. However, this is a quite different condition than the PHE failure event postulated to occur in a LFR system.

The kind of interfacial contact between the two fluids occurred in Sibamoto et al. experiments does not happen when superheated liquid water is injected inside a hot molten metal pool. It is concluded that the condition for the triggering of unstable boiling of the accumulated water is not well understood yet. If T_i is the interface temperature and T_{HN} is the temperature of homogeneous nucleation, the consequence of the liquid-liquid contact would be more energetic for $T_i > T_{HN}$ than for $T_i < T_{HN}$. The consequence depends also on the amount of water brought into contact with the melt and the coherence of the contact.

The water jet, by going from the exit plane pressure to the lead pool pressure enters the two-phase region. Downstream of the exit plane there is flashing and a jet expansion region, where the jet width increases, and the liquid fragments into droplets. The formation of a steam bubble around water droplets is favourable when the injection orifice is about 0.1 mm or less. As a matter of fact, for these dimensions, the trapped water droplets are kept physically separated from hot lead, precluding the possibility of steam explosion. For steam explosion to happen water droplets should be heated through direct contact with lead droplets at a rate higher than the maximum possible rate of heat absorption by droplet evaporation, converting most of the energy transferred to superheating the water. In this case, the rate of energy exchange between the water and the lead droplets is so high that little time is given to water droplets to evaporate. When the superheated water is suddenly converted to vapor, a steam explosion occurs, and a shock wave is generated. However, this mixing mechanism is highly unlikely to happen during the PHE failure event since water droplets are significantly diluted in the depressurized two-phase water mixture.

IV. REACTOR-SCALE SIMULLATIONS

IV.A. Code usage rationale

RELAP5 is a flexible code that allows modelling complex geometry domains in multiphase. Among additional features, it has choked flow models. Furthermore it is relatively fast and output files are lightweight. The code was extensively validated and used for water-cooled systems. A modified version[41] of the code, improved by University of Pisa to model liquid metal systems, is used in this paper. The thermodynamics and thermo-physical properties of lead implemented[42] are those recommended by the Nuclear Energy Agency (NEA) Handbook on Lead-bismuth Eutectic Alloy and Lead properties, materials compatibility, thermal-hydraulics and technologies[43]. For a given system only one working fluid and non-condensable gases (NCGs) are allowed. Since NCGs thermodynamic properties have been found inadequate to perform equivalent gas injections, SIMMER-III was used to find the transient boundary conditions. SIMMER-III is a general two-dimensional, three-velocity-field, multiphase, multicomponent, Eulerian, fluid-dynamics code[44]. On the other hand, it is not suitable to simulate complex, non-axisymmetric geometries and simulations take significantly longer than RELAP5. It takes longer to run a few seconds long SIMMER-III simulation than to run a several hours long RELAP5 simulation, and the memory usage is also order of magnitudes greater. SIMMER-III has the capability to simulate liquid metal-water interaction and has been expanded for heavy liquid coolant applications[45]. Steam generator tube ruptures in LFRs are most commonly studied in SIMMER-III[46]. Experimental campaigns to study heavy liquid metal-water interaction (i.e. Pb, PbLi, LBE) have been done, and the pressure trends predicted by the code are in good agreement with experimental data[31].

IV.B. RELAP5/MOD3.3 Westinghouse LFR simulations

A RELAP5/MOD3.3 model was developed for the Westinghouse LFR. The reactor is subdivided in three systems: the primary, the secondary and the passive heat removal system. Three PHE failure scenarios are analysed: a middle failure ("midF" failure at the middle of a primary channel, half of the air is injected into the HP and half into the UCP), an end failure in the HP ("endF in HP" failure at the end of a primary channel on the HP side (inlet); it is assumed that the secondary fluid blowdown happens only in the HP) and an end failure in UCP ("endF in UCP" failure at the end of a primary channel on the UCP side (outlet); it is assumed that the secondary fluid blowdown happens only in the UCP).

The initial conditions are obtained from a steady state run. Starting from lead at 390 °C, power is given to the reactor core and water is circulating in PHEs, while the cover gas pressure is fixed at 1.1 bar. Steady state results are in good agreement with the nominal conditions. Velocities inside the core are below the recommended limit of 2 – 3 m/s to avoid significant erosion of structures and components[47]. Overall pressure drops in the primary loop are relatively low and during normal operation the power lost from the RV to outside is a small percentage (about 0.1 %) of the nominal power.

To obtain the transient boundary conditions the same geometry (a simple closed cylinder partially filled with lead and the injection channel located in the centre) was modelled in RELAP5/MOD3.3 and SIMMER-III. In the SIMMER-III domain the secondary channel is filled with water at 350 bar and 340 °C, while the lead pool is at

530 °C and the cover gas at 1.1 bar. After 0.1 seconds the channel is connected to the pool and the injection takes place. SIMMER-III was used to determine the boundary conditions (0.975 kg/s for 1.3 seconds at 206 bar and 530 °C) for the equivalent NCG injection in the RELAP5/MOD3.3 simulations. The criteria used to find the boundary conditions was to obtain the same pressurization in both codes, injecting a NCG in RELAP5/MOD3.3 and injecting water in SIMMER-III.

Let us consider the PHE model, connected on one side to the HP and on the other to the UCP. To model the failure, the primary system is put in communication with the secondary system. For a middle-failure two time dependent volumes (TMDPVOLs) and two time dependent junctions (TMDPJUNs) are used to set up the NCG equivalent injection, while for the end failures only one of each is necessary (Figure 4). In any case the total NCG equivalent mass flow rate is set to 0.975 kg/s and the duration of the injection is set to 1.3 s, 3 s, and 5 s.

[FIGURE 4 GOES HERE]

The reactor is kept isothermal at 530 °C. Isothermal conditions are a good approximation due to the short transient duration. After 10000 seconds of steady state, the equivalent NCG flow rate is imposed, going from 0 kg/s at t = 9999.9 s to 0.975 kg/s at t = 10000.0 s. 500 seconds before the injection the connection to the TMDPVOL responsible for maintaining constant the reactor cover gas pressure is closed, so that the primary system remains isolated. When using a TMDPJUN a look-up-table has to be defined and, since the code cannot handle steep ramps, it is not possible to reproduce the pressure wave in the very early phase of the transient.

[FIGURE 5 GOES HERE]

Figure 5 shows the pressurization in the reactor cover gas region for a middle failure, highlighting the difference for various injection durations. Such trends are representative of all three failure modes (middle and end failures). The same pressure trend is observed in each case and the final steady state pressure is quite similar (within a 0.3 bar interval).

The maximum pressure variation at the base of HP and UCP for all the modes of failure and injection times is 2.65 bar which is less than the lead hydrostatic pressure, while the maximum lead level variation is 108 mm, less than the cove gas height (Figure 6 shows a typical lead level trend in the HP. There is an initial peak, which is promptly damped. The lead returns to the initial level in about 20 s).

[FIGURE 6 GOES HERE]

These pressure values are an upper bound estimate. This upper bound do not pose a threat to the integrity of the RV and internals, but the seals of the core top plugs could experience a leakage of cover gas (without significant radioactive products release). In reality, the cover gas pressure regulation and relief system, here not considered, regulates the pressure, and the expected pressure will be lower than the computed one, avoiding this release.

V. LEAD-SH2O INTERACTION TESTING FACILITY

The PHE failure testing facility will help to understand the phenomenology of the WEC LFR PHE failure and to validate computer codes. The facility will be used to assess the water mass flow rate during blowdown (measured either by weighting the vessel containing the water to be injected before and after the test using load cells or by using Fast Pressure Transducers (FPTs) to evaluate the instantaneous water mass flow rate), the liquid lead sloshing occurrence and associated forces (measured with FPTs) and the two phase water jet impingement load on the vessel wall (measured with FPTs).

Because the FPTs signal drifts severely with time, the experiment should not last longer than a few seconds, including the time to fail the rupture cap and subsequent blowdown. An alternative could be the adoption of a custom device made of a thin circular metal plate. It would be clamped to a cylindrical support fixed to the vessel wall, with a strain gauge positioned on top of the thin plate. Such a device might be ineffective if the magnitude and duration of the sloshing force is not large enough. The strain gauge should move in response to a force, displacing the surrounding lead. But, due to its virtual mass, such movement is difficult to occur. Due to the high inertia of the molten lead, to accelerate the plate into the plastic regime the required plate thickness could be too small. Figure 7 shows the Process Flow Diagram of the facility.

[FIGURE 7 GOES HERE]

There are five vessels in the facility. The injection takes place in an Interaction Vessel (IV), which is partially filled with pure lead at nearly atmospheric pressure (1.1 bar) and the injected water comes from a Water Vessel (WV), pressurized at 350 bar. To limit the pressurization of the IV and thus its pressure rating a Dump Vessel (DV), always in communication with the IV, is used. The DV can act as an expansion vessel if filled with inert gas or as a quenching tank if partially filled with water. To provide the IV with molten lead, lead ingots are melted in a Melting Tank (MT) through a multi-batch approach and the melted metal is transferred to a Storage Tank (ST), used to drain/fill the IV.

For the WV design, priority was given to a simpler layout and operation of the facility. Due to spatial constraints, a smaller WV made of a 2 m long 4 inches pipe was chosen. This means that the WV experiences a higher depressurization during the transient, however (as long as the pressure remains above the saturation pressure to avoid flashing) smaller cover gas volume is better for indirectly measuring the injected mass with a FPT. Furthermore, since the vessel is to be weighted to determine the mass of water left in the vessel after the injection, a smaller vessel is desirable. For the chosen configuration, a discharge of subcooled water at 350 bar and 340 °C causes the pressure inside the WV to drop to 292 bar, while a discharge of supercritical water at 350 bar and 415 °C causes an even lower depressurization due to the lower choked flow rate.

The IV and the DV are always in communication and each one is provided with a rupture disk designed to rupture at 50 bar and 15 bar (see Sections V.A and V.B) respectively. All the lines where lead is expected to flow are heated to 380 °C to prevent blockage due to lead freezing.

The IV volume was determined according to the specifications provided by WEC, while the WV volume comes from consideration of space constraints and ease of operation of the facility. Table III summarizes the estimated vessels volumes.

[TABLE III GOES HERE]

The injection line runs from the WV to the IV. It is a modular line, made of two sections: a shorter and smaller capillary tube to reproduce the PHE secondary channel and a longer and larger capillary tube, to reproduce the PHE primary channel. The smaller section is the one connected to the WV. The experimental investigation will consider failure of one and three PHE channels. For both configurations, the flow area is evaluated to account for the flow coming from both sides of a PHE channel.

The long capillary tube has a rupture "disk" (cap) at the end, that should fail quickly at the desired pressure (Figure 8).

[FIGURE 8 GOES HERE]

For this purpose, testing is required to calibrate the depth of the notch on the cap. The tube will be initially filled with SCW. Due to the early stage of the research on this topic, a large conservatism is assumed in the definition of the experimental campaign. In fact, high-pressure gas bubbles will be discharge into the lead pool, which will expand and occupy a significant volume of the lead pool. It will cause sloshing forces in the IV much larger than those expected in the reactor vessel. This is acceptable as the measured sloshing forces will be conservative, although not prototypical.

The absence of a primary heat exchanger mock-up in the testing facility is explained by the manufacturing process of the PCHE. Such heat exchanger has a monolithic construction, like a solid block. Thus, unlike what would normally be done for a steam generator tube rupture experiment, investigation of the impact of a single channel failure on adjacent channels is not needed.

Based on considerations on the lead virtual mass, it is decided to rely only on FPTs to measure the blowdown impingement force and the sloshing force. Two FPTs are foreseen on the vessel bottom, two on the vessel walls, one at the bottom of the WV, one at the top of the WV, and one just before the capillary tube.

To capture the interaction between SCW and lead an IV model was developed with SIMMER-III. It can handle more than one working fluid and it tracks complex fluid motions. On the other hand, a model of the DV and a portion of the dump line was developed with RELAP5/MOD3.3 because of the non-axisymmetric geometry, the presence of a single fluid and the lower computational effort required. To determine the boundary conditions for the RELAP5/MOD3.3 model, the first section of dump line connected to the IV is included in the SIMMER-III model.

V.A. Interaction Vessel SIMMER-III simulations

The IV volume is fixed at 0.08 m3 (upper bound value proposed by WEC). A vessel internal diameter of 0.44 m and a height of 0.526 m are assumed. The injection tube corresponding to a three channel failure is considered in the numerical investigation, a most severe scenario (see Table IV for the tube dimensions). A series of configurations have been analysed. A nodalization scheme of the SIMMER-III model referring to the last configuration considered can be seen in Figure 9. The IV is originally modelled as a closed vessel to assess response of the vessel with no venting. Such configuration is referred as V1 in the following discussion. The assumed initial condition is 530 °C and 1.1 bar (cover gas pressure) in the IV, and 340 °C and 350 bar in the injection tube.

The water temperature and pressure are imposed at the uppermost water channel cell (cell [1;119] in Figure 9). During the experiments the pressure in the IV is not expected to drop below 292 bar. After 0.1 seconds the water channel is opened (the virtual wall is set to be open) and the water blowdown starts.

[TABLE IV GOES HERE]

[FIGURE 9 GOES HERE]

The response of the lead pool and the gas phase expansion were investigated. The case matrix is shown in Table V. V1 runs are characterized by the closed vessel where only the water temperature and pressure are imposed as boundary condition. Different initial lead temperature and argon cover gas volume are analysed.

[TABLE V GOES HERE]

Figure 10 shows the effect of increasing the lead temperature within the IV, comparing the outcomes of 1-V1, 2-V1, and 3-V1. In each case, the inlet mass flow rate is calculated by SIMMER-III. It should be noted that SIMMER-III does not have the choked flow model. The plot shows the IV pressure (solid lines) and the injected mass flow rate (dotted-dashed lines) vs. the problem time. The water injection starts at 0.1 s, reaching the maximum value of around 1.75 kg/s in 10 ms. The calculated maximum flow rate is the same for the three simulations. Following the water injection, pressure starts to increase, with initial oscillations. In the first 0.1 s after the beginning of the injection, the three simulations show a similar pressure increase. After that, the IV pressure increases faster for higher initial lead temperature. The water mass flow rate remains constant for the first 0.3 s. Then, as the IV pressure increases, the water flow rate decreases. As expected, the water flow rate is lower for higher IV pressures (thus for higher initial lead temperature). At the end of the simulation (1 s after the beginning of the injection) a maximum pressure of around 200 bar is obtained for the worst case. These are upper bound values, and the calculations will be refined in the next phase of the computational campaign.

[FIGURE 10 GOES HERE]

Simulation outcomes highlight some issues related to the operation of the IV in the configuration V1. A strong pressurization (about 160 bar in 1 second) is observed within the IV. It calls attention to the importance of maintaining the open flow path to the DV (configuration V2 in the following). The DV acts as a quenching tank, limiting the pressurization in the IV. The V2 configuration was reproduced with SIMMER-III by adding a portion of the dump line to the V1 model. To minimize the computational cost, the DV is replaced with a boundary condition, imposing a fixed pressure of 1.1 bar at the end of the dump line. This boundary condition is equivalent to an infinite volume DV.

Figure 11 compares the cases 2-V1 and 1-V2, plotting the injected mass flow rate (dotted-dashed lines) and the IV pressure (solid lines) vs. problem time. In the first 0.1 seconds after the beginning of injection, pressure peaks are observed, and their magnitudes are much greater in 1-V2 (up to 559 bar against a maximum of about 40 bar in 2-V1). From a close-up inspection of the output file, these peaks are localized and are presumably due to the lead impinging on the IV's flange (contact pressure). As the lead reaches the top of the IV, such numerical peaks are observed travelling radially in single isolated cells. In 2-V1 the peaks are much smaller due to the damping action of the cover gas, as it has no escape path. The dump line should stay clear of lead deposition and blockage to secure passage of gases. However, a significant pool swelling is observed and the dump line is obstructed. The mass flow rate in 2-V1 decreases with time due to the continuous pressurization of the IV, while in 1-V2 it stays nearly constant (about 1.75 kg/s) thanks to the much lower pressurization due to the dump line. The lower pressurization also causes the mass flow rate in run 1-V2 to be significantly higher compared to run 2-V1. It shows how the presence of the dump line is critical in keeping the pressure in the IV low (about 15 bar for 1-V2 against more than 200 bar for 2-V1).

[FIGURE 11 GOES HERE]

Previous calculations were performed by imposing the calculated injection rate to the code. Nevertheless, the calculated injection rate is observed to be much higher than the expected one (choked flow). For the choked flow condition, the expected injection rate is 0.52 kg/s. Hence, calculation 1-V2 was repeated (2-V2) by imposing the velocity of the injected water to match the choked flow value. In Figure 12 pressure and water mass flow rate trends against time are plotted for imposed temperature and pressure (black lines; please, refer to the online version of the paper for colours) and for imposed fluid velocity (red lines). The much lower flow rate determines a strong pressure difference in the cover gas between the two runs. With the evolution of the transient after about 1.5 seconds the pressure trends tend to converge toward a value below 10 bar. In both cases, lead reaches the IV lid, and a significant amount of fluid ends up in the dump line. This is due to the sloshing motion, being too intense relative to the IV size. Figure 13 shows the lead flow rate through the dump line. In run 2-V2 329.9 kg of lead out of an initial inventory of 672.5 kg are expelled after 1.6 s of injection.

[FIGURE 12 GOES HERE]

[FIGURE 13 GOES HERE]

The dump line obstruction is a highly undesirable phenomena since it leads to the blockage of the pressure relief. A solution to lead entrainment in the dump line is placing a plate just before the dump line entrance. Such configuration is referred as the V3 configuration. The diameter of the plate is two times that of the dump line, while the flow area between the IV lid and the plate is 10 times the flow area of the dump line. A new simulation was run with the same initial and boundary conditions as the V2 calculation. The expected result was not obtained; in the run 1-V3 obstruction of the dump line took place in the same way as V2 runs.

Further modifications to the model were made. In the hereinafter referred to as V4 configuration, the long capillary tube was extended to 50 mm from the bottom of the vessel instead of 250 mm in V2. To provide more head space for steam and to limit the pressurization the lead pool height was lowered to 400 mm instead of 426 mm in V2. Moreover, the ID of the short capillary tube was reduced to 0.5 mm from 2.55 mm in V2. Still, no changes in the overall phenomena were observed. There was a significant swelling of the pool and liquid lead reached the top of the IV, causing plugging of the dump line. To limit the bubble generation due to flashing of water in the injection tube, the configuration V5 was developed, reducing the long capillary tube ID from 7.82 mm to 4.51 mm.

Figure 14 shows a pressure trend comparison between run 2-V4 (solid black line) and run 2-V5 (solid red line). A smaller long capillary tube means that less water is initially discharged inside the IV. Thus, for run 2-V5 the pressurization in the first 1.25 seconds of simulation is smaller (about 2 bar instead of 3) and less lead is expelled from the IV in that time. In fact, in run 2-V4, after 2 seconds of simulation, 236 kg of lead are expelled, while in run 2-V5 only 177 kg leave the IV.

[FIGURE 14 GOES HERE]

The modifications proposed in the model V5 do not solve the problem of lead plugging the dump line. Sloshing motions are still intense and not representative of what is expected at reactor scale. A small capillary tube does not seem like a practical path to pursue, both from a manufacturing point of view and from the results obtained with the SIMMER-III code. If the failure opening is to be further reduced a possible solution might be to use a plate with a pin-hole drilled through it and place it upstream the long capillary tube. Furthermore, a bigger IV and/or a lower lead pool depth could be considered. The appropriate pool depth could be investigated experimentally by gradually increasing the depth from one experiment to the next. Anyhow, a IV pressure rating of 50 bar should be sufficient for the current design of the vessel, regardless of whether the capillary tube size is that considered in V2, V4 or V5.

Figure 15 shows evolution of the pool swelling in the run 2-V5. The images represent a radial section of the IV, with the injection line in the centre and the dump line in the top right. Initially the injection line is filled with water (light blue), while the vessel contains lead (red) and argon (white) at rest. The green region is a no calculation zone and no material is located in it. At the start of the transient a steam (also white) bubble is generated just outside the injection tube, while inside the tube fluid is still entirely liquid. Then, the pressure in the channel decreases and the water flashes inside the long capillary tube, while it remains liquid in the short one. The steam bubble increases in size until the dump line is plugged by lead. When the dump line is partially cleared, the steam bubble decreases in size and detaches from the bottom of the vessel. From the exit plane a two-phase flow discharge takes place and in the long capillary tube there is also liquid water. Several steam bubbles are formed while in the injection tube the liquid water/steam interface moves up until almost all the liquid phase is concentrated in the upper region of the long capillary tube. Initially the pressure in the lower region of the vessel where the steam bubble grows is higher than the rest of the vessel but after some fractions of a second the pressure in the entire vessel reaches similar values.

[FIGURE 15 GOES HERE]

V.B. RELAP5/MOD3.3 Dump Vessel simulations

The Dump Vessel can be used as a quenching tank or as an expansion vessel. In quenching tank mode, the DV is partially filled with water and the mixture coming from the IV is discharged under the water. The purpose of the quenching tank is to condense the discharged steam and reduce the pressure in the dump vessel. On the other hand, in the expansion vessel mode, the DV is filled with steam and NCGs.

A series of RELAP5/MOD3.3 simulation was done to investigate the pressurization inside the vessel for two DVs of different volumes. The main geometrical parameters are reported in Table VI.

[TABLE VI GOES HERE]

Figure 16 shows the nodalization scheme of the facility. The TMDPVOL 1 fixes the steam temperature, while the TMDPJUN 2 imposes the steam mass flow rate. Two parallel PIPEs (10 & 20), connected with multiple cross junctions, are used to simulate the lower part of the DV (water region). This approach allows a better mixing of the fluid.

[FIGURE 16 GOES HERE]

The injection lasts 10 seconds (experiments will be shorter due to the WV size and FPTs signal drift), with an initial mass flow rate ramp of 0.1 s and a final ramp of 0.5 s. The amount of initial water in the DV must guarantee a complete condensation of steam. More water within the DV will mean less available gas volume for damping the pressurization. The opposite is true if there is less water at a higher temperature. For the simulations half of the DV is filled with water. Conservatively it is assumed that all the water exiting the injection channel in the IV vaporizes instantly to the lead temperature in the IV and is expelled to the dump line, even though this is not the actual phenomenon according to SIMMER-III simulations. Thus, a steam mass flow rate of

0.52 kg/s is imposed at the entrance of the dump line. The dump line is kept at 380 °C while different steam temperatures have been investigated. A coupling between the RELAP5/MOD3.3 and the SIMMER-III simulations would allow for a more realistic evolution of the transient. Such kind of work was done by Galleni et al.[48] and by Gonfiotti et al.[49] to study the interaction between molten lead lithium alloy and water.

After 10000 s of steady state in the DV at 1.1 bar the injection starts with a flow rate from 0 to 0.52 kg/s in the time interval 10009.9 – 10010.0 s. In Figure 17 the pressure trends in the DV cover gas for injections of steam at 415, 530 and 630 °C in the 500 l and in the 750 l DV are shown. The different temperatures and volumes have been investigated to assess the capability of the DV to condense steam and limit pressurization. For all the cases an initial pressure peak lasting about 1.6 s can be seen. The smaller the DV, the higher the pressure during the injection phase, especially the initial peak caused by the hot gas followed by steam blowdown at the start of the transient. The gas bubble migrates toward the cover gas and a pressure plateau at approximately 1.3 bar is reached after the first peak. This latter pressure response is due to the steam flow into the DV. The subsequent pressure reduction (after around 10 s) is due to steam condensation. Shortly after the injection ends and steam is condensed at about 10020.5 s no residual pressurization is observed. The pressure always remains well below the design pressure (15 bar).

The water temperature experiences an initial peak (from 30 °C to a maximum of 45 °C) at the start of the injection, followed by a linear increase for the duration of the injection. As expected, the final temperature of water for smaller vessel volumes and for higher steam temperatures is higher (45 °C for steam at 650 °C in the 500 l DV against

39 °C for steam at 415 °C in the 750 l DV). Decreasing the original amount of water in DV causes a higher final temperature.

[FIGURE 17 GOES HERE]

In Figure 18 the pressure trend at the dump line entrance is shown. There is an initial peak at the start of the injection, lasting about 0.5 s and reaching 6.8 bar. For the remaining part of the blowdown a plateau at about 4.4 bar is established.

To investigate the use of the DV as an expansion vessel, simulations have been done in the 750 litres model by removing water and substituting it with argon at 380 °C. A pressure of 12 bar has been obtained for 4.9 s of injection of steam at 415 °C, for 4.0 s of injection of steam at 530 °C and for 3.5 s of injection of steam at 630 °C. Accounting for a safety margin of 1.25 and for the fact that an injection longer that 3.5 seconds is unlikely to be made due to the pressure drop in the WV and FPTs signal drift, a 750 l DV with a design pressure of 15 bar is proposed, so that it can be used in both modes.

[FIGURE 18 GOES HERE]

VI. CONCLUSIONS

Experiments have been done to study the injection of water into molten lead, however, the specific conditions of the WEC LFR have not been tested yet. The PHE failure in the WEC LFR has been simulated and the preliminary design of the PHE failure testing facility has been developed to investigate the phenomena involved. RELAP5/MOD3.3 and SIMMER-III computational codes were used. The separate effect test facility will be used also to produce experimental data for the validation of the computational tools.

RELAP5/MOD3.3 reactor-scale simulations of the WEC LFR have been done by considering equivalent NCG conditions. Results show very limited consequences due to the failure: the pressurization in the primary system is lower than the lead hydrostatic pressure and the maximum lead pool level variation is below 110 mm. Lead level oscillations are promptly damped.

A testing facility layout including instrumentation list, vessels, and process flows is proposed. Vessel volumes and design pressures were evaluated to scale the reactor behaviour. The interaction inside the vessel is very intense and further design activity is planned: a smaller rupture area or a lower lead level should be investigated. The latter can be accomplished by increasing the lead level incrementally and observing the response of the lead pool and pressures in each experiment. The proposed DV is capable to operate either as a quenching tank or as an expansion vessel.

A coupling between RELAP5/MOD3.3 and SIMMER-III will allow more realistic simulation of the transient. In the present analysis with SIMMER-III a fixed pressure is imposed at the end of the dump line. The coupling will synchronize the timestep, and the boundary condition will be updated at each timestep to take into account the feedback from both codes. This can be done by devising a coupling procedure.

[1] M. FRIGNANI et al., “ALFRED: A Strategic Vision for LFR Deployment”, *Nuclear Science and Engineering*, **117**, 1468 (2022).

[2] H. A. ABDERRAHIM et al., “MYRRHA–A multi-purpose fast spectrum research reactor”, *Energy conversion and management*, **63** (2012).

[3] A. ALAMBERTI et al., “ALFRED reactor coolant system design”, *Nuclear Engineering and Design*, **370** (2020); https://doi.org/10.1016/j.nucengdes.2020.110884.

[4] V. NARCISI et al., “Preliminary evaluation of ALFRED revised concept under station blackout”, *Nuclear Engineering and Design*, **364** (2020); https://doi.org/10.1016/j.nucengdes.2020.110648.

[5] J. WALLENIUS, “SEALER: a small lead-cooled reactor for power production in the Canadian Arctic”, *Proc. Int. Conf. on Fast Reactors and Related Fuel Cycles: Next Generation Nuclear Systems for Sustainable Development*, Yekaterinburg, Russian Federation, 26-29 Jun 2017, IAEA-CN--245-431.

[6] World Nuclear News; https://world-nuclear-news.org/Articles/Construction-licence-issued-for-Russias-BREST-reac (current as of Oct. 1, 2022).

[7] Powermag; https://www.powermag.com/press-releases/rosatom-completes-foundation-concreting-for-the-brest-od-300-reactor/ (current as of Oct. 1, 2022).

[8] Y. WU, “Design and R&D Progress of China Lead-Based Reactor for ADS Research Facility”, *Engineering*, **2**, *1*, 124 (2016); https://doi.org/10.1016/J.ENG.2016.01.023.

[9] *RELAP5/MOD3.3 CODE MANUAL VOLUME II: APPENDIX A INPUT REQUIREMENTS. NUREG/CR-5535/Rev P3-Vol II App A*, Information Systems Laboratories, Inc. (2006).

[10] *SIMMER-III (Version 3. F) Input Manual*, O-arai Engineering Center,Japan Nuclear Cycle Development Institute, May (2012).

[11] P. FERRONI et al., “The Westinghouse Lead Fast Reactor: design overview and update on development activities”, presented at the International Conference on Fast Reactors and Related Fuel Cycles, Vienna, Austria, April 19-22, 2022.

[12] J. LIAO et al., “Development of phenomena identification and ranking table for Westinghouse lead fast reactor's safety”, *Progress in Nuclear Energy*, **131** (2021); https://doi.org/10.1016/j.pnucene.2020.103577.

[13] G. MUSGROVE, R. LEPIERRES, J. NASH, “Heat exchangers for supercritical CO2 power cycle applications”, 4th International Symposium on Supercritical CO2 Power Cycles, Pittsburgh, Pennsylvania, United States, 9-10 Sept. 2014.

[14] N. BARTEL et al., “Comparative analysis of compact heat exchangers for application as the intermediate heat exchanger for advanced nuclear reactors”, *Annals of Nuclear Energy*, **81**, 143 (2015); https://doi.org/10.1016/j.anucene.2015.03.029.

[15] P. RAVINDRAN, P. SABHARWALL, N. A. ANDERSON, “Modeling a printed circuit heat exchanger with relap5-3d for the next generation nuclear plant”, INL/EXT-10-20619, Idaho National Laboratory (Dec. 2010).

[16] X. LI, “Alloy 617 for the high temperature diffusion-bonded compact heat exchangers”, *Proc. Of ICAPP, Anaheim, CA, USA, 8-12 Jun 2008*

[17] S. A. WRIGHT et al., “Summary of the Sandia Supercritical CO_2 Developmnet Program”, presented at SCO2 Power Cycle Symposium, Boulder, Colorado, USA, May 24-25, 2011.

[18] A. P. SIMANJUNTAK, J. Y. LEE, “Mechanical Integrity Analysis of a Printed Circuit Heat Exchanger with Channel Misalignment”, *Applied Sciences*, **10**, 2169 (2020); https://doi.org/10.3390/app10062169.

[19] S. R. AAKRE, I. W. JENTZ, M. H. ANDERSON, “Nuclear code case development of printed-circuit heat exchangers with thermal and mechanical

performance testing", presented at the Sixth International Supercritical CO2 Power Cycles Symposium, Pittsburgh, Pennsylvania, United States 27-29 March 2018.

[20] S. K. MYLAVARAPU et al., "Fabrication and design aspects of high-temperature compact diffusion bonded heat exchangers", *Nuclear Engineering and Design*, **249**, 49 (2012).

[21] B. SUNDEN, "High temperature heat exchangers (HTHE)", Proc. of the 5th International Conference on Enhanced, Compact and Ultra-Compact Heat Exchangers: Science, Engineering and Technology, Hoboken, NJ, USA, September 2005.v

[22] Y. LEE, J. I. LEE, "Structural assessment of intermediate printed circuit heat exchanger for sodium-cooled fast reactor with supercritical CO2 cycle", *Annals of Nuclear Energy*, **73**, 84 (2014); https://doi.org/10.1016/j.anucene.2014.06.022.

[23] K. N. SONG, S. D. HONG, "Structural integrity evaluation of a lab-scale PCHE prototype under the test conditions of HELP", *Science and Technology of Nuclear Installations*, 2013; https://doi.org/10.1155/2013/520145.

[24] Y. MIZOKAMI et al., "Development of structural design procedure of plate-fin heat exchanger for HTGR", *Nuclear Engineering and Design*, **255**, 248 (2013); https://doi.org/10.1016/j.nucengdes.2012.09.013.

[25] Vpei, https://www.vpei.com/

[26] V. DOSTAL, M. J. DRISCOLL, P. HEJZLAR, "A supercritical carbon dioxide cycle for next generation nuclear reactors" (2004)

[27] Heatric, https://www.heatric.com/

[28] M. T. FARMER et al., "Design of a test facility to investigate fundamental Na-CO2 interactions in compact heat exchangers", ANL-GENIV-164). Argonne National Laboratory (Sept. 2010).

[29] M. EPSTEIN, S. J. LEE, “UK-BEIS Advanced Modular Reactor Phase 2 Project: Primary Heat Exchanger Failure Test Matrix”, WGS-UK-00192-RPT-0003, Rev. A, Westinghouse Electric Company (2021).

[30] M. EPSTEIN, “WGS-UK-00192-RPT-0004 – UK-BEIS Advanced Modular Reactor Phase 2 Project: Evaluation of Steam Explosion Due to Accidental Supercritical Liquid Water Discharge from PHE into Molten Lead Pool”, WGS-UK-00192-RPT-0004, Rev. 0, Westinghouse Electric Company (2021).

[31] P. LORUSSO et al. "GEN-IV LFR development: status & perspectives.", *Progress in Nuclear Energy*, **105**, 318 (2018); https://doi.org/10.1016/j.pnucene.2018.02.005

[32] F. J. MOODY, “Introduction to unsteady thermofluid mechanics”, *Wiley-Interscience*, 1990.

[33] P. L. KIRILLOV, G. P: BOGOSLOVSKAYA, “Heat and mass transfer in nuclear power plants”, *Energoatomizdat Publ.*, 2000

[34] B. S. PETUKHOV, “Handbook for Thermohydraulic Calculations”, *Énergoatomizdat Publ.*, **1**, 1987.

[35] A. V. BEZNOSOV et al., “Experimental studies of the characteristics of contact heat exchange between lead coolant and the working body”, *Atomic Energy*, **98**, 170 (2005).

[36] A. CIAMPICHETTI et al., “Experimental and computational investigation of LBE–water interaction in LIFUS 5 facility”, *Nuclear Engineering and Design*, **239**, *11*, 2468 (2009); https://doi.org/10.1016/j.nucengdes.2009.08.007.

[37] A. DEL NEVO et al., “Experimental Campaign in Support of the Safety Studies of the STGR in LFR”, *Proc. 18th International Topical Meeting no Nuclear Reactor Thermal Hydraulics (NURETH 2019)*, Portland, OR, USA, August 18-23 2019.

[38] M. EBOLI et al., “Characterization of leak detection in HLM system using ‚LIFUS5/MOD3 facility”, *Proc. 18th International Topical Meeting no Nuclear Reactor Thermal Hydraulics (NURETH 2019)*, Portland, OR, USA, August 18-23 2019.

[39] P. SHEN et al., “Corium behavior and steam explosion risks: A review of experiments”, *Annals of Nuclear Energy,* **121**, 162 (2018); https://doi.org/10.1016/j.anucene.2018.07.029.

[40] Y. SIBAMOTO, Y. KUKITA, H. NAKAMURA, “Small-scale experiment on subcooled water jet injection into molten alloy by using fluid temperature-phase coupled measurement and visualization”, *Journal of nuclear science and technology*, **44**, *8*, 1059 (2012).

[41] G. BARONE, D. MARTELLI, N. FORGIONE, “Implementation of Lead-Lithium as working fluid in RELAP5/Mod3. 3”, *Fusion Engineering and Design*, **146**, 1308 (2019).

[42] P. BALESTRA et al., “New RELAP5-3D Lead and LBE Thermophysical Properties Implementation for Safety Analysis of Gen IV Reactors”, *Science and Technology of Nuclear Installations* (2016)

[43] C. FAZIO et al., “Handbook on lead-bismuth eutectic alloy and lead properties, materials compatibility, thermal-hydraulics and technologies-2015 edition”, NEA—7268, Nuclear Energy Agency of the OECD (NEA), 2015.

[44] Y. TOBITA et al., “The development of SIMMER-III, an advanced computer program for LMFR safety analysis, and its application to sodium experiments”, *Nuclear Technology*, **153**, *3*, 245 (2006).

[45] S. WANG et al., “Evaluation of a steam generator tube rupture accident in an accelerator driven system with lead cooling”, *Progress in Nuclear Energy*, **50**, 363 (2008); https://doi.org/10.1016/j.pnucene.2007.11.018

[46] X. HUANG et al., "Numerical investigation on LBE-water interaction for heavy liquid metal cooled fast reactors", *Nuclear Engineering and Design*, 361 (2020); https://doi.org/10.1016/j.pnucene.2018.02.005[47] M. FROGHERI, M. ALEMBERTI, L. MANSANI, “The Advanced Lead Fast Reactor European Demonstrator (ALFRED)”, *Proc. the 15th International Topical Meeting on Nuclear Reactor Thermal-Hydraulics, NURETH-15*, Pisa, Italy, May 12-17 2013.

[48] F. GALLENI et al., “RELAP5/SIMMER-III code coupling development for PbLi-water interaction”, *Fusion Engineering and Design*, **153** (2020); https://doi.org/10.1016/j.fusengdes.2020.111504.

[49] B. GONFIOTTI et al., “Development of a SIMMER\RELAP5 coupling tool”, *Fusion Engineering and Design*, **146**, 1993 (2019).

Table I. Key input data used for the calculations

Parameter	Value	Unit
Lead core inlet T	390	°C
Lead core outlet T	650	°C
PHE water inlet T	340	°C
Core power	950	MW_{th}
Primary loop pressure	1.1	bar
Secondary loop pressure	350	bar
Total lead mass flow rate	24900	kg/s
Core geometry	Proprietary information	-
Core peaking factors	Proprietary information	-
RV and internals approximate geometry	Proprietary information	-
PHE channels geometry	Proprietary information	-

Table II. Summary of experimental evidence of water injection into liquid lead/LBE

Paper	Water pressure	Water temp.	Melt	Melt pressure	Melt temp.	Injection mode	Mass flow rate	Nozzle ID	Energetic interaction
	Bar	°C	-	Bar	°C	-	g/h	mm	-
Beznosov et al., 2005 (Ref. 35)	100-250	100-350	Lead		350-600	Water into melt		0.6-10	No
	30	200	Lead		360-390	Water into melt	30	1	No
	220-240	150-250	Lead		500-600	Water into melt			No
Ciampichetti et al., 2008 (Ref. 36)	70	235	LBE	1	350	Water into melt		4	No
Del Nevo et al., 2019 (Ref. 37)	180	270	LBE	2	400	Water into melt	2.36 kg/s max (nozzle ID 12.6 mm)	4; 8.9; 12.6	No
Eboli et al., 2019 (Ref. 38)	19.3-20.3	170-247	LBE	1	203-246	Water into melt		0.04-0.2	No
	20.1	219	LBE	1	226	Water into melt	394	0.0637	No

Wang et al., 2008 (Ref. 45)	70	235	LBE	1	340	Water into melt			No
Sibamoto et al., 2007 (ref. 40)		25-90	LBE		230-550	Water on melt pool surface		6	Yes

Table III. Vessels volumes

Component	**Volume (l)**
IV	80
WV (P_{final} = 292 bar, height = 2 m)	16.22
DV (P_{design} = 15 bar) as an expansion volume	670.2
ST	25.30

Table IV. SIMMER-III V1 model geometry, BC & IC

Parameter	**Value**	**Unit**
Short capillary tube ID	2.55	mm
Short capillary tube length	60	mm
Long capillary tube ID	7.82	mm
Long capillary tube length	50	mm
Injection plane distance from IV bottom	250	mm

Table V. SIMMER-III simulations matrix

		Water boundary conditions				
Run ID	**Model**	**T_{H2O} (°C)**	**p_{H2O} (bar)**	**Γ_{H2O} (kg /s)**	**T_{Pb} (°C)**	**Notes**
1-V1	V1	340	350	-	415	
2-V1	V1	340	350	-	530	
3-V1	V1	340	350	-	630	
4-V1	V1	415	350		415	
5-V1	V1	340	350	-	530	+ 50 % argon volume

6-V1	V1	340	350	-	530	+ 100 % argon volume
1-V2	V2	340	350	-	530	
2-V2	V2	-	-	0.58	530	
1-V3	V3	340	350	-	530	
1-V4	V4	340	350	-	530	
2-V4	V4	-	-	0.022	530	
1-V5	V5	340	350	-	530	
2-V5	V5	-	-	0.022	530	

Table VI. DV sizing parameters

Parameter	**500 l DV**	**750 l DV**	**Unit**
Tank internal diameter	0.752	0.83	m
Water level from the vessel's bottom	0.56	0.646	m
Dump line length (outside the vessels)	3.5	3.5	m
Injection plane distance from the bottom of the vessel	100	100	mm

Figure 1. Westinghouse LFR flow path (notional representation)

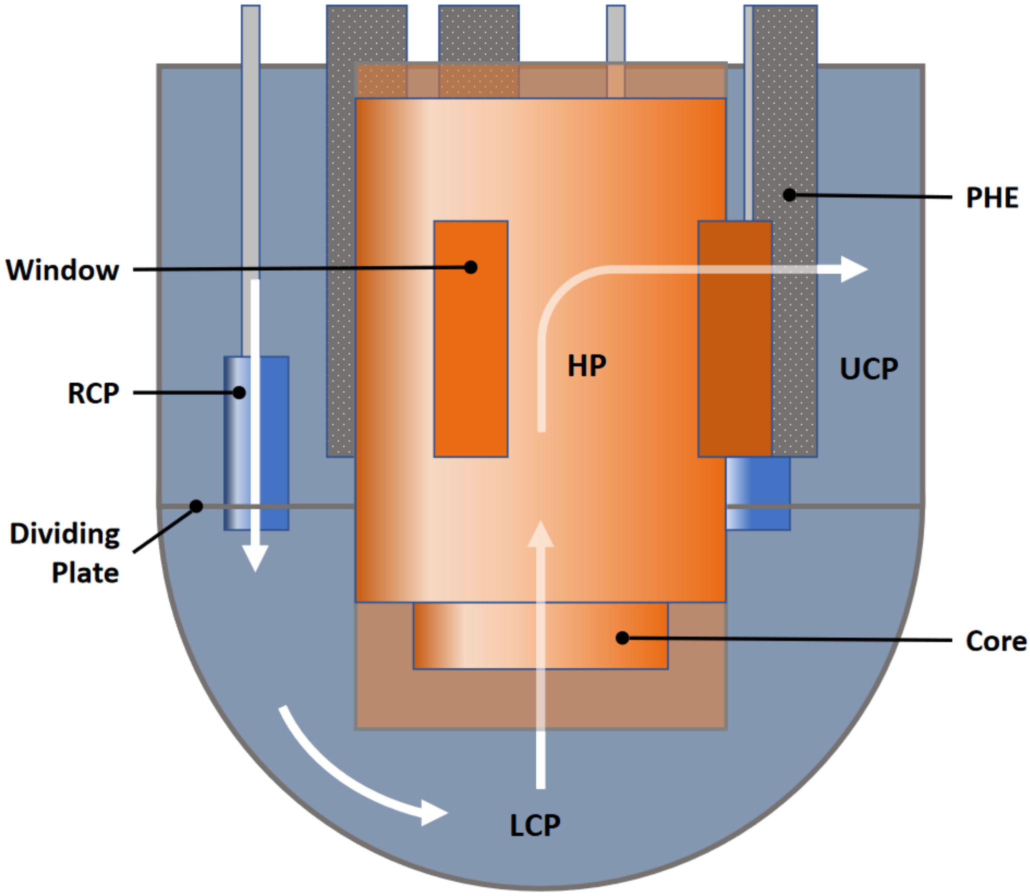

Figure 2. PHE channel failure: 1) shock wave in primary channel propagating away from the failure location; 2) shock wave spreading over a hemisphere when it reaches the UCP; 3) spherical shock wave just before il reaches the reactor vessel wall[29]

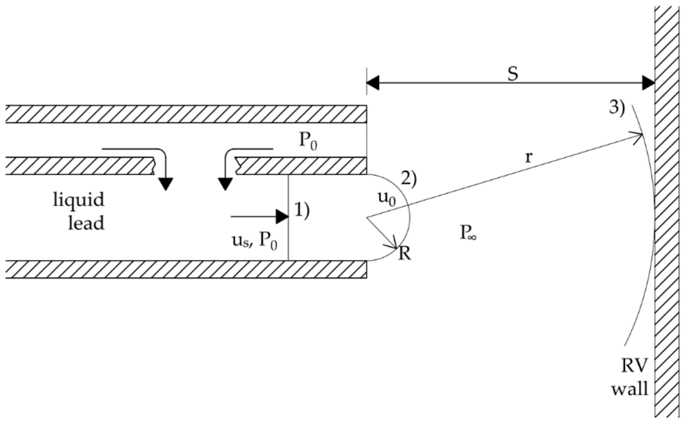

Figure 3. LIFUS5 facility injection system[38]

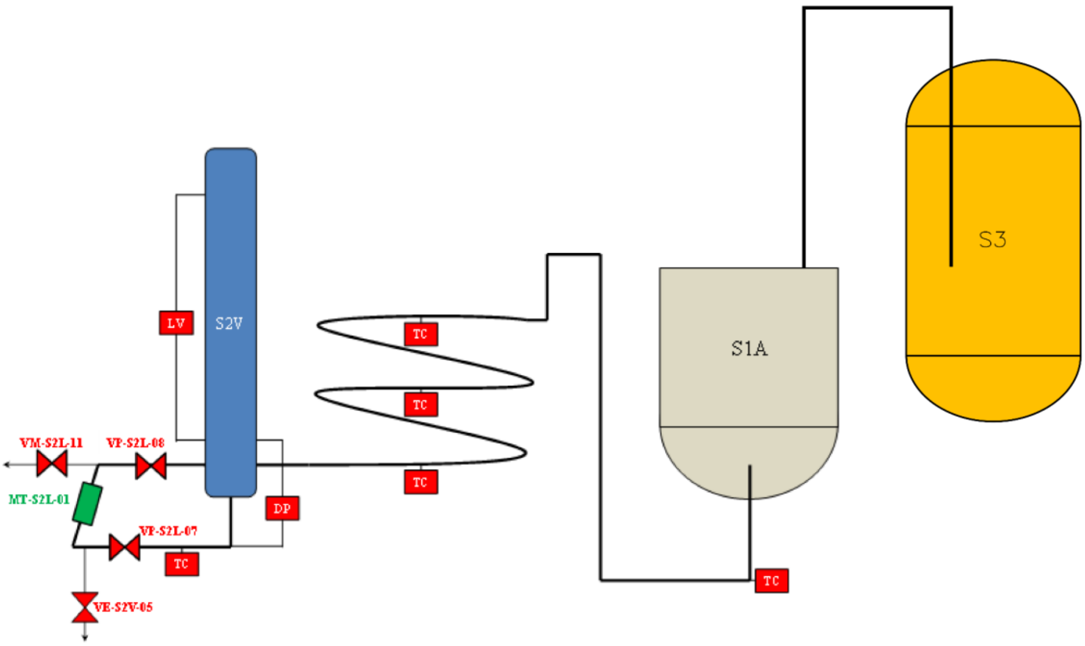

Figure 4. PHE RELAP5/MOD3.3 nodalization

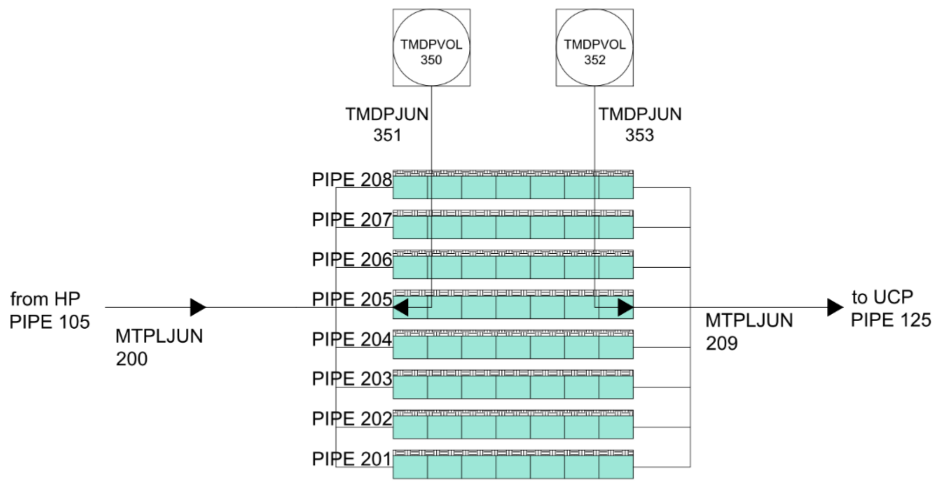

Nuclear Technology (2023) DOI: 10.1080/00295450.2023.2173482

Figure 5. pressure trend in cover gas – middle failure

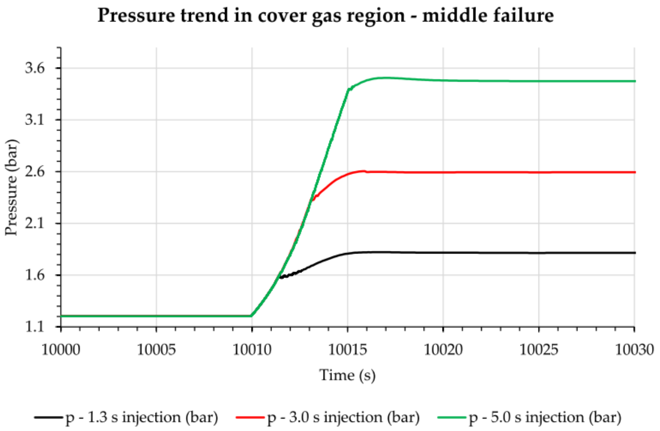

Figure 6. lead level variation in HP

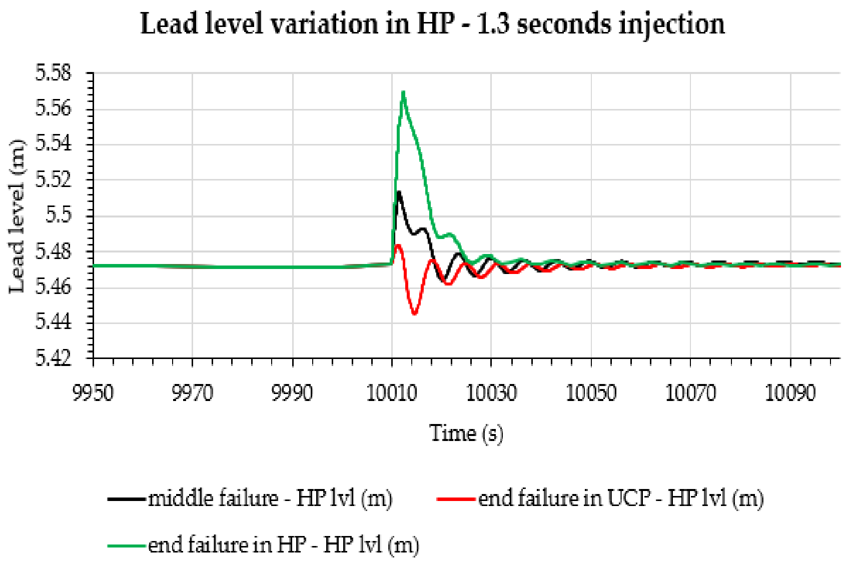

Nuclear Technology (2023) DOI: 10.1080/00295450.2023.2173482

Figure 7. PHE Failure Testing Facility Process Flow Diagram

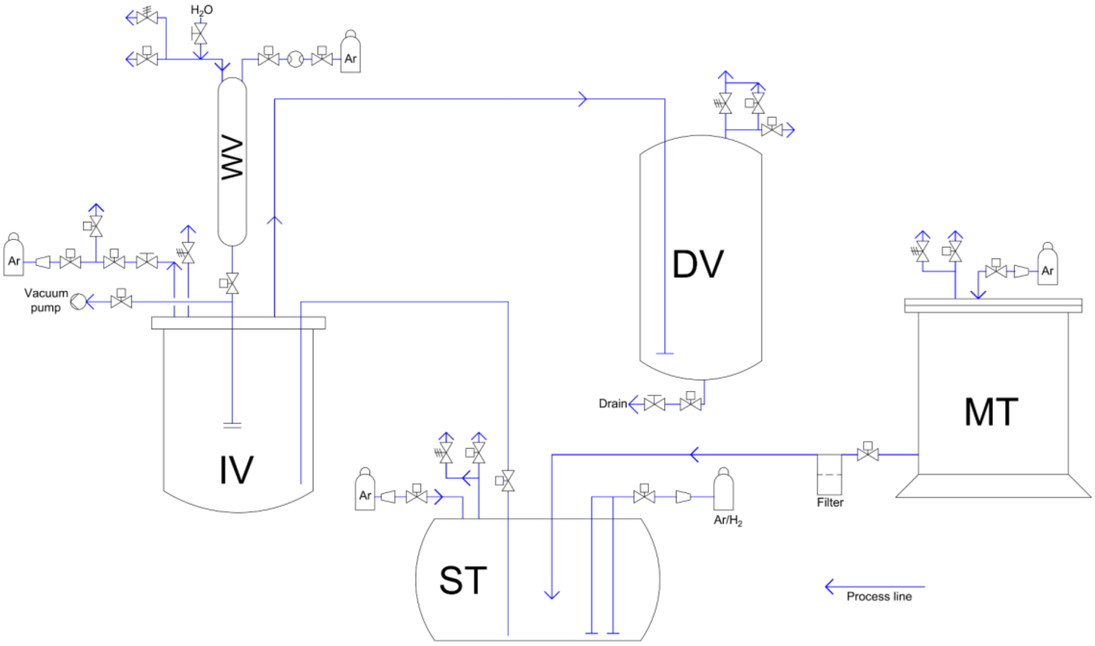

Figure 8. Injection channel notational representation (not in scale)

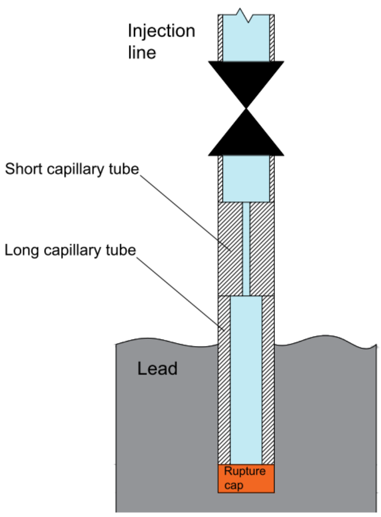

Figure 9. IV SIMMER-III nodalization, configuration V5

Nuclear Technology (2023) DOI: 10.1080/00295450.2023.2173482

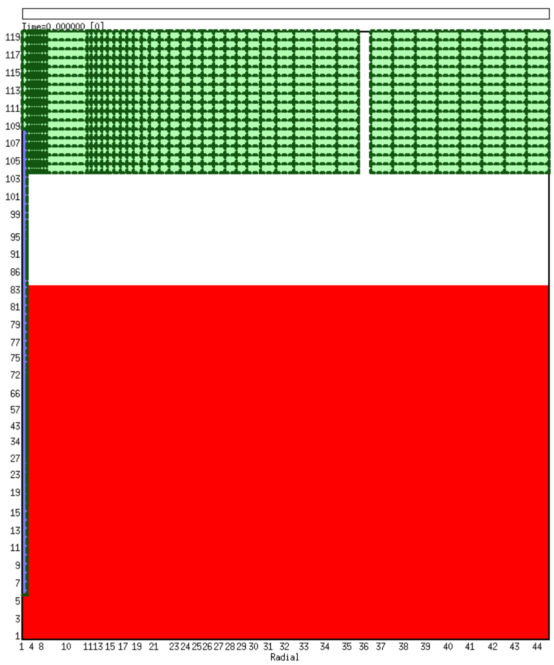

Figure 10. Effect of increasing lead pool temperature

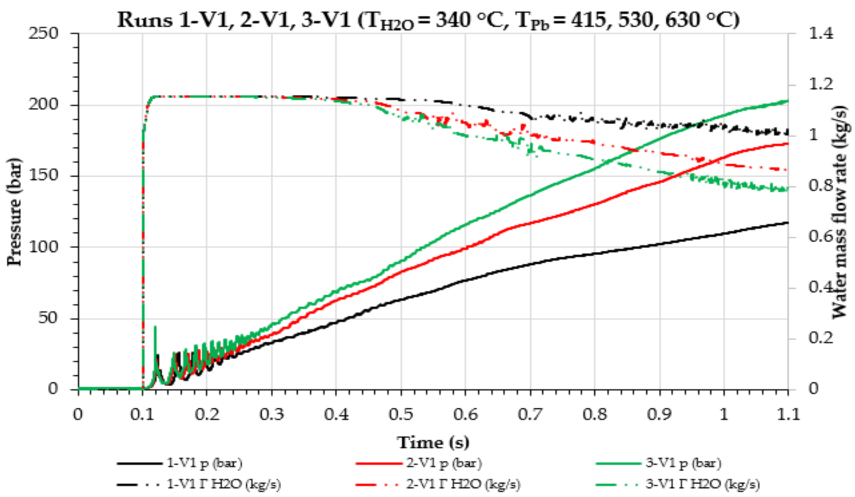

Figure 11. Effect of the dump line presence

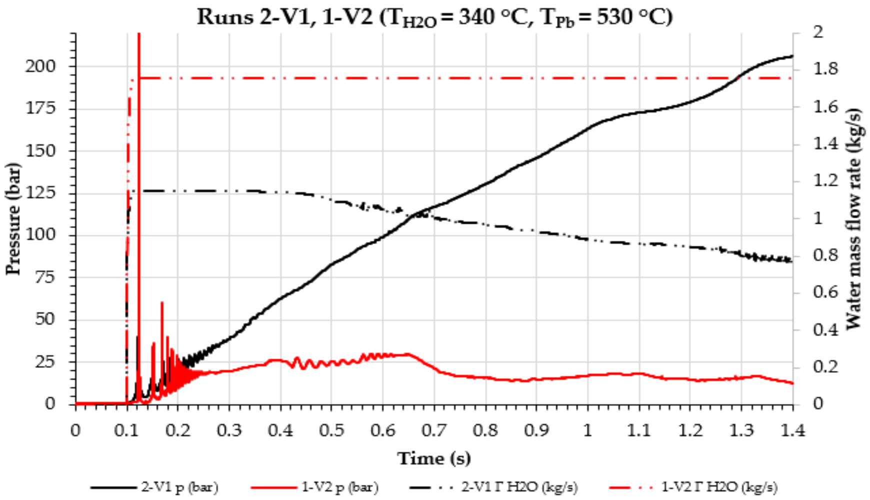

Figure 12. Fixed water velocity as boundary condition

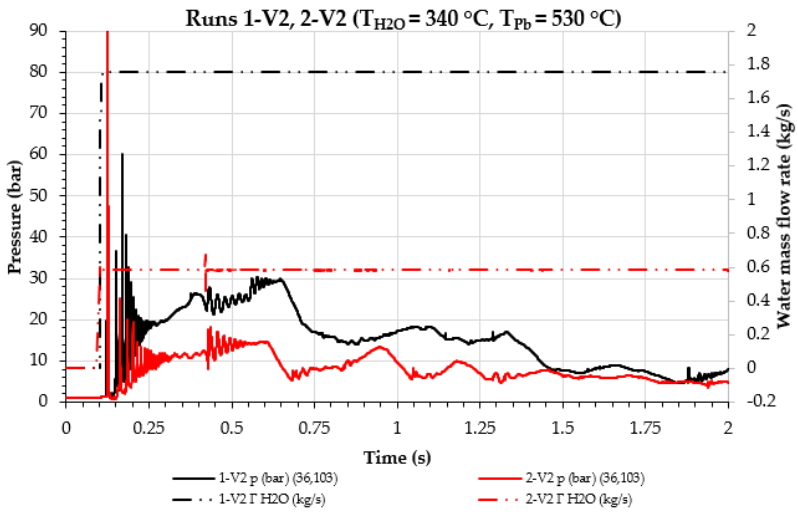

Figure 13. Lead mass flow rate through the dump line, Runs 1-V2 and 2-V2

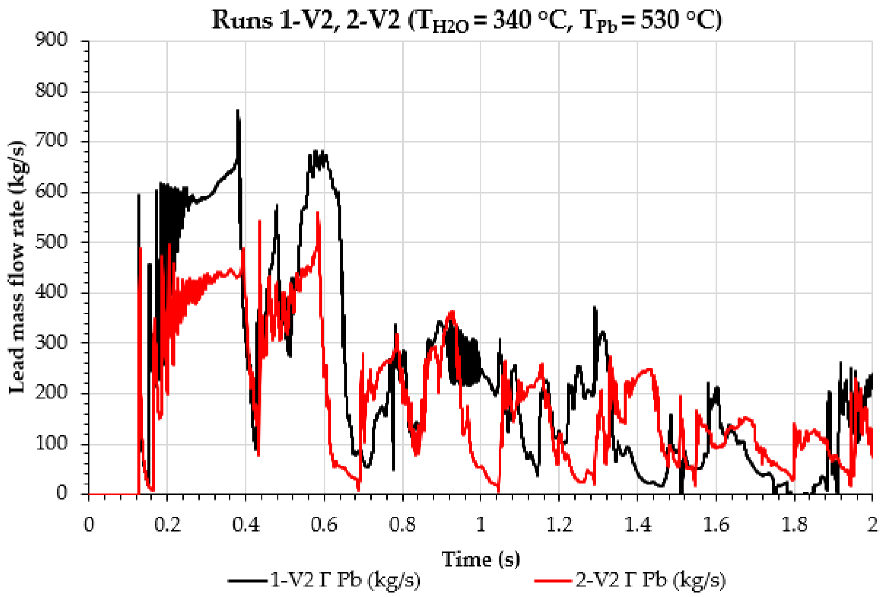

Figure 14. Runs 2-V4 and 2-V5 pressure trends

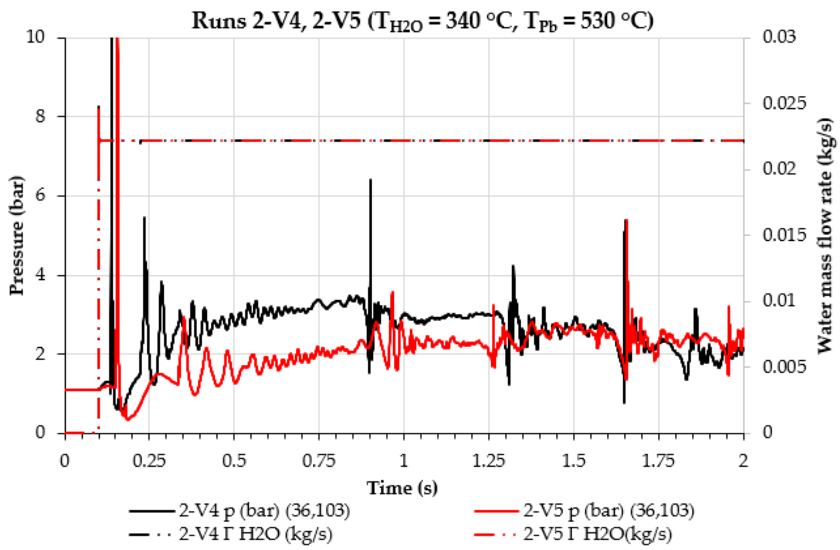

Figure 15. Run 2-V5 evolution – material distribution

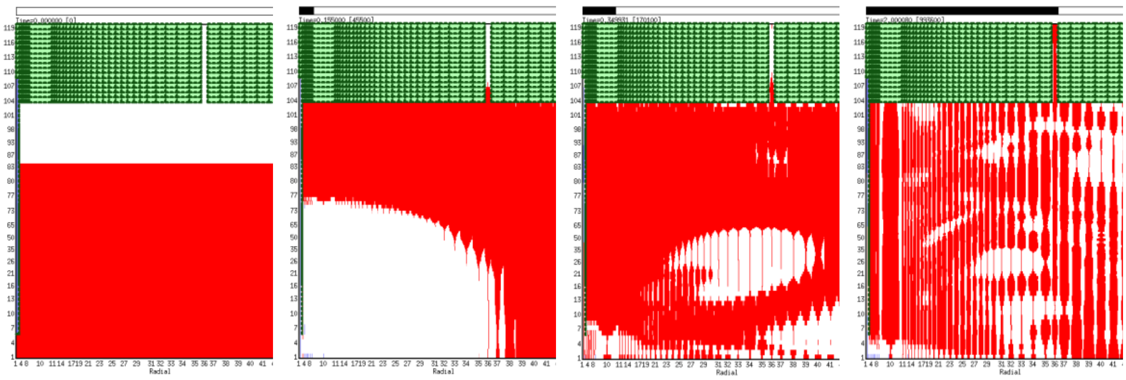

Figure 16. 750 liters Dump Vessel RELAP5/MOD3.3 nodalization

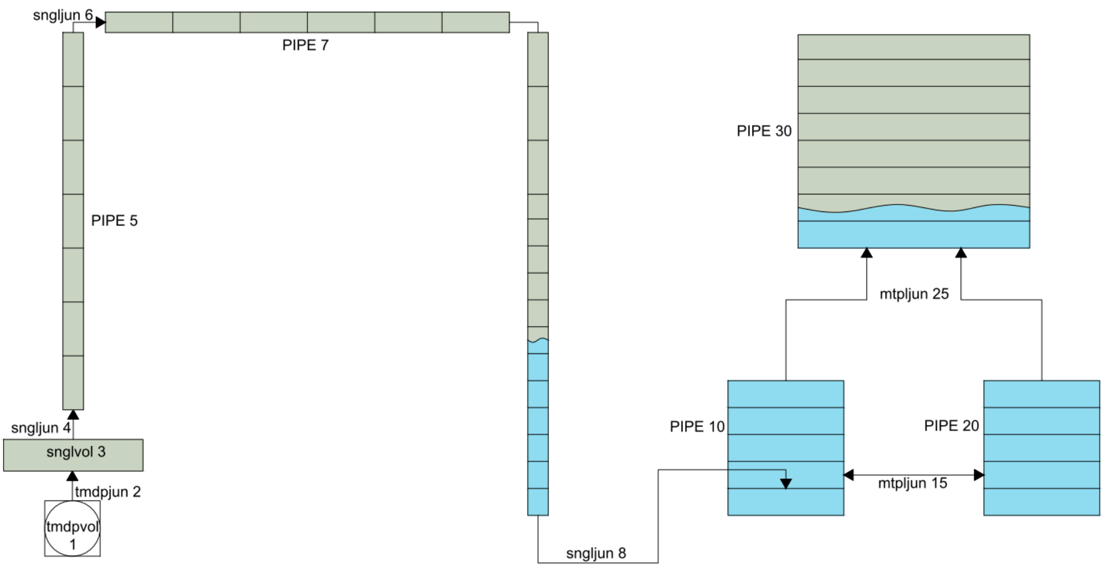

Figure 17. Pressure in the DV cover gas

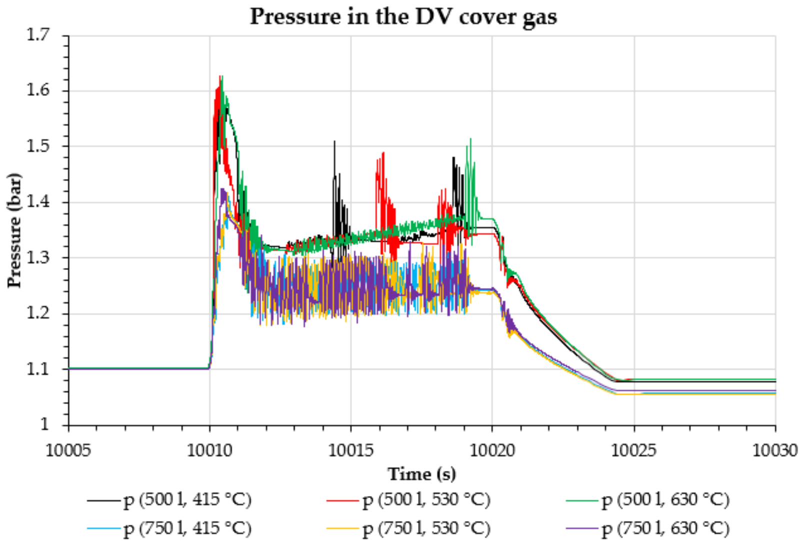

Figure 18. Pressure at the entrance of the dump line